REPORTS

OPTICS

Observation of optical polarization Möbius strips

Thomas Bauer,[1,2] Peter Banzer,[1,2,3] Ebrahim Karimi,[3]* Sergej Orlov,[1,2] Andrea Rubano,[4,5] Lorenzo Marrucci,[4,5] Enrico Santamato,[4] Robert W. Boyd,[3,6] Gerd Leuchs[1,2]

Möbius strips are three-dimensional geometrical structures, fascinating for their peculiar property of being surfaces with only one "side"—or, more technically, being "nonorientable" surfaces. Despite being easily realized artificially, the spontaneous emergence of these structures in nature is exceedingly rare. Here, we generate Möbius strips of optical polarization by tightly focusing the light beam emerging from a *q*-plate, a liquid crystal device that modifies the polarization of light in a space-variant manner. Using a recently developed method for the three-dimensional nanotomography of optical vector fields, we fully reconstruct the light polarization structure in the focal region, confirming the appearance of Möbius polarization structures. The preparation of such structured light modes may be important for complex light beam engineering and optical micro- and nanofabrication.

Interference is one of the most intriguing features of the wave nature of light. This phenomenon can give rise to points or lines of zero intensity, when three or more plane waves are superimposed. Around these "nodes," the phase of the optical beam undergoes a dislocation, determined by the beam's wavelength as well as the geometry of the optical system (*1*). The phase variation around these points is described by a topological charge ℓ, an integer that determines the number of 2π phase cycles along a path around these nodes (*2*). The phase of the optical field is undefined at these nodes, and thus, such points are called phase singularities (*3*). Complex superpositions of optical beams result in rich topological structures of phase and intensity. For instance, elaborate beams designed by a computer-generated hologram form dark lines and knots in 3-dimensional (3D) space upon propagation (*4*, *5*). In addition, the vectorial features of multibeam interference lead to interesting polarization topologies (*6*–*8*). Three main polarization topologies—"lemon," "star," and "monstar"—are invoked in the paraxial regime to describe the vectorial patterns in the plane transverse to the beam propagation direction (*9*, *10*). A general polarization topology can be generated by a coherent superposition of two nonplanar circularly polarized beams with opposite handedness, copropagating paraxially and possessing nonidentical topological charges:

$$\mathbf{E}(\mathbf{r}) = \cos\left(\frac{\Theta}{2}\right) \mathrm{LG}_{p_1,\ell_1}(\mathbf{r})\mathbf{e}_\mathrm{L} + \sin\left(\frac{\Theta}{2}\right) e^{i\chi} \mathrm{LG}_{p_2,\ell_2}(\mathbf{r})\mathbf{e}_\mathrm{R} \qquad (1)$$

where Θ and χ respectively define amplitude coefficients and the relative phase between the two different polarization states; $\mathbf{e}_\mathrm{L}$ and $\mathbf{e}_\mathrm{R}$, are unit vectors of left- and right-hand circular polarization; and $\mathrm{LG}_{p,\ell}(\mathbf{r})$ are Laguerre-Gaussian (LG) modes with radial and azimuthal indices p and ℓ (*11*). The polarization of these beams in the transverse plane samples the entire Poincaré sphere, and the beams are thus called Poincaré beams (*12*). Two main polarization singularities, C-points and L-lines, respectively denoting points of circular and lines of linear polarization, are used to describe the beams' polarization topology (*13*, *14*).

In 2005, a beam configuration was proposed that consists of a pair of noncoaxial circularly

[1]Max Planck Institute for the Science of Light, Guenther-Scharowsky-Strasse 1, D-91058 Erlangen, Germany. [2]Institute of Optics, Information and Photonics, Friedrich-Alexander-University Erlangen-Nuremberg, Staudtstrasse 7/B2, D-91058 Erlangen, Germany. [3]Department of Physics, University of Ottawa, 25 Templeton Street, Ottawa, Ontario K1N 6N5, Canada. [4]Dipartimento di Fisica, Università di Napoli Federico II, Complesso Universitario di Monte Sant'Angelo, via Cintia, 80126 Napoli, Italy. [5]Consiglio Nazionale delle Ricerche (CNR)–SPIN, Complesso Universitario di Monte Sant'Angelo, via Cintia, Napoli, Italy. [6]Institute of Optics, University of Rochester, Rochester, NY 14627, USA.
*Corresponding author. E-mail: ekarimi@uottawa.ca

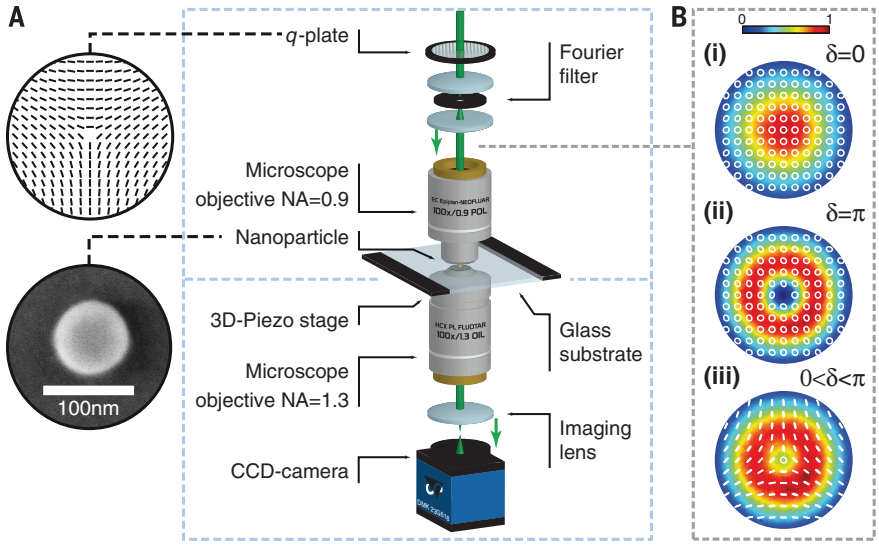

Fig. 1. Schematic of the experimental apparatus, and the intensity and polarization patterns of the generated beams. (**A**) A mode-cleaned right-hand circularly polarized TEM_{00} mode laser beam at a wavelength of 530 nm is sent through a $q = -1/2$-plate (QP). A spatial Fourier filter, made of two lenses and a pinhole, is used to filter unwanted higher-order radial modes of the generated beam after the QP. This beam is a superposition of a right-hand circularly polarized TEM_{00} mode and a left-hand circularly polarized $\mathrm{LG}_{0,1}$ mode, in which the superposition ratio was carefully adjusted by means of an external voltage applied to the QP. The composite beam is tightly focused by a microscope objective with a NA of 0.9 onto a single spherical gold nanoparticle with a diameter of 82 nm, sitting on a glass substrate. A 3D piezo stage is used to scan the sphere within the focal plane. The transmitted light is collected by an oil-immersion objective with NA = 1.3. A camera combined with an imaging system is used to image the back focal plane of the lower microscope objective for each position of the nanoparticle in the focal plane. Top and bottom insets respectively show the orientation of liquid crystal molecules in the $q = -1/2$-plate and a scanning electron microscope image of the gold nanoparticle. (**B**) Measured intensity and polarization distributions of the optical beam emerging from the QP. The local polarization ellipse is superimposed onto the intensity distribution in white color. The three cases (i) to (iii) correspond to different optical retardations, realized by applying different voltages to the QP: (i) a pure right-hand circularly polarized TEM_{00} beam, (ii) a pure left-hand circularly polarized $\mathrm{LG}_{0,1}$ beam, and (iii) a superposition of (i) and (ii). In the latter case, however, the beam possesses a polarization topology of –1/2 in the form of a star with a C-point on the optical axis.

polarized beams of opposite handedness with different scalar topological charges. In this scheme, a nonparaxial 3D polarization topology is generated at the beams' intersection plane (*15*). Analytical calculations revealed spectacular 3D-polarization topologies in the form of twisted ribbons and Möbius strips (*16*). Möbius strips are 3D objects that possess only a single surface and a single boundary component (*17*, *18*) and have been observed in chemistry, biology (*19*), particle physics (*20*), and materials science (*21*–*23*). In our experiment, these 3D objects are created by the tight focusing of individual Poincaré beams, as given by Eq. 1, by exploiting the longitudinal field component appearing in the focal region. In order to visualize the polarization Möbius strip, we reconstructed the amplitudes and relative phases of the individual components of the electric field and traced the polarization ellipse around the optical axis in the focal plane.

The optical element we used to generate the Poincaré beam is a *q*-plate, a patterned, birefringent plate with optical retardation δ and made of nematic liquid crystal. The orientation of the principal axis of the liquid crystal molecules comprising the *q*-plate varies with the azimuthal coordinate, so that the structure possesses a topological charge q (*24*). When $\delta = \pi$, the *q*-plate flips the handedness of the spin of an incoming beam and adds an orbital angular momentum (OAM) of $|2q|$ to the outgoing beam. For a non-π retardation, the *q*-plate generates a Poincaré beam from a circularly polarized Gaussian input beam. The generated beam is a coherent superposition of the fundamental TEM_{00} ($LG_{0,0}$) and $LG_{0,\pm 2q}$ modes with opposite circular polarizations, as described by Eq. 1 for $p_1 = p_2 = \ell_1 = 0$ and $\ell_2 = \pm 2q$. The optical retardation of the *q*-plate and its orientation determine the amplitude of the superposition coefficients, Θ, and relative phase between the two beams, χ, respectively (*10*). Our experiment involves a Poincaré beam with a polarization topology of $q = -1/2$ (or $q = -3/2$), and we tune the mode ratio between the two aforementioned modes by varying δ using an applied voltage (*25*). The intensity and polarization distributions of the output beam in the near-field of a *q*-plate with $q = -1/2$ are presented in Fig. 1B, for different optical retardations.

A star-shaped Poincaré beam with a polarization topology of −1/2 (Fig. 1B, iii), produced by the *q*-plate, is tightly focused by a microscope objective with a numerical aperture (NA) of 0.9, producing a complex focal field distribution, with a spot size comparable with the wavelength of the light beam. The paraxial approximation does not hold under tight focusing conditions, and the beam in general is no longer transverse as a strong longitudinal component of the electric field is created (*26*). We hence have $\mathbf{E} = E_x\hat{\mathbf{x}} + E_y\hat{\mathbf{y}} + E_z\hat{\mathbf{z}}$, where E_i are the components of electric field, and $\hat{\mathbf{x}}$, $\hat{\mathbf{y}}$, and $\hat{\mathbf{z}}$ are the unit vectors in a Cartesian coordinate frame in which z is oriented as the beam axis. In the present case, the strengths of the electric field components $|E_i|$ are almost the same. Furthermore, the intensity distribution close to the focus is highly asymmetric, and the initial cylindrical symmetry is broken into one of its subgroups—namely, the dihedral D_3 group. The symmetry-breaking observed in the beam intensity arises from the preexisting threefold symmetry of the initial beam's transverse polarization distribution. Shown in Fig. 2A are the theoretically calculated electric energy density and phase distributions of individual components of the electric field E_x, E_y, and E_z of the tightly focused Poincaré beam and the total electric energy density distribution at the focus (*26*).

We used a nanoprobe-based reconstruction technique to experimentally probe and reconstruct the electric field distributions generated in the focal plane, allowing the optical polarization Möbius strips hidden in this complex field structure to be observed (*27*). For this technique, we used a spherical gold nanoparticle on a glass substrate and scanned it through the field under study (Fig. 1A). The scattered and transmitted light was collected and angularly resolved for each position of the nanoprobe relative to the field distribution by using an immersion-type microscope objective with NA = 1.3. This procedure allows for the reconstruction of both amplitude and phase distributions from the data recorded for each nanoprobe position relative to the beam in the focal plane and different effective observation directions (*10*, *27*). The experimentally reconstructed intensity and relative phase distributions of the three individual electric field components of the tightly focused beam are shown in Fig. 2B. Because of the spin-to-OAM conversion, the longitudinal z-component of the field gains additional OAM of ±1, with the sign depending on the helicity of the input beam polarization (*28*). The beam is highly asymmetric because of its nonparaxiality.

We used the approach introduced in (*29*) to trace out the 3D orientation of the polarization

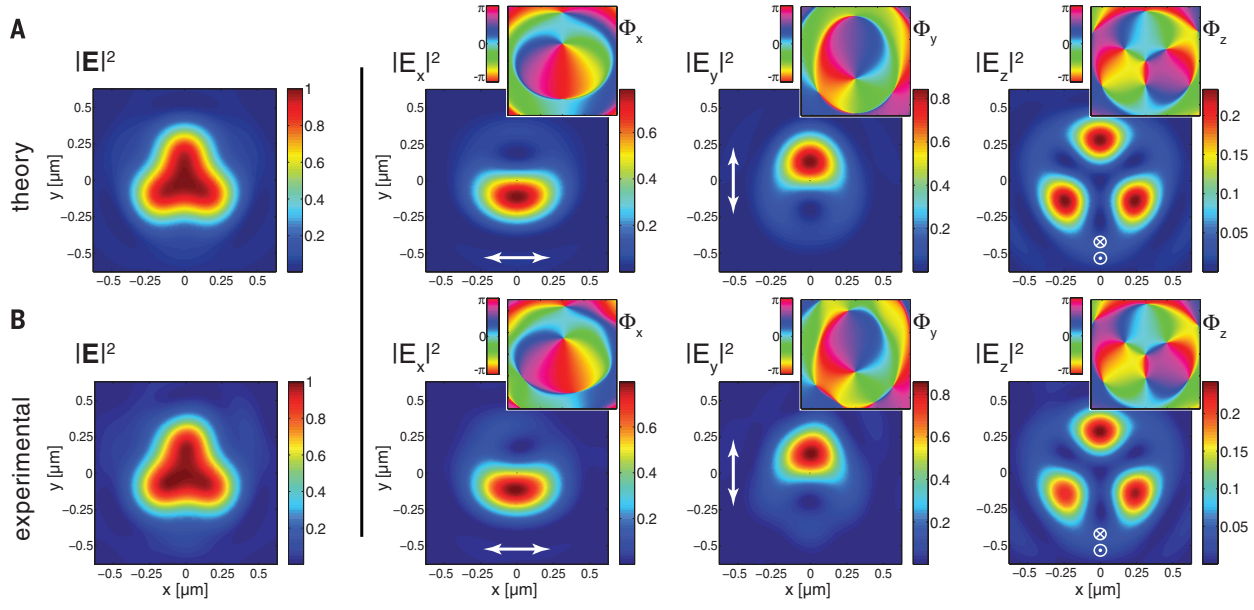

Fig. 2. Numerically calculated and experimentally observed electric energy density distributions of a tightly focused Poincaré beam. (**A**) and (**B**) show the numerically calculated and experimentally measured total electric energy density distribution as well as the electric energy densities and phase distributions of the individual field components of the tightly focused Poincaré beam shown in Fig. 1B, iii, in the focal plane of the high-numerical-aperture objective. Under tight-focusing conditions, the beam loses its cylindrical symmetry. Moreover, a longitudinal component of the field is generated. Top-right insets show the corresponding phase patterns for each field component, Φ_x, Φ_y, and Φ_z. Because of spin-to-OAM conversion, the longitudinal field component gains a helical phase-front of $\exp(\pm i\varphi)$, with a sign that depends on the input beam polarization. Three separated phase vortices can be seen surrounding the beam axis, generated by the interference of the two constituent input beams.

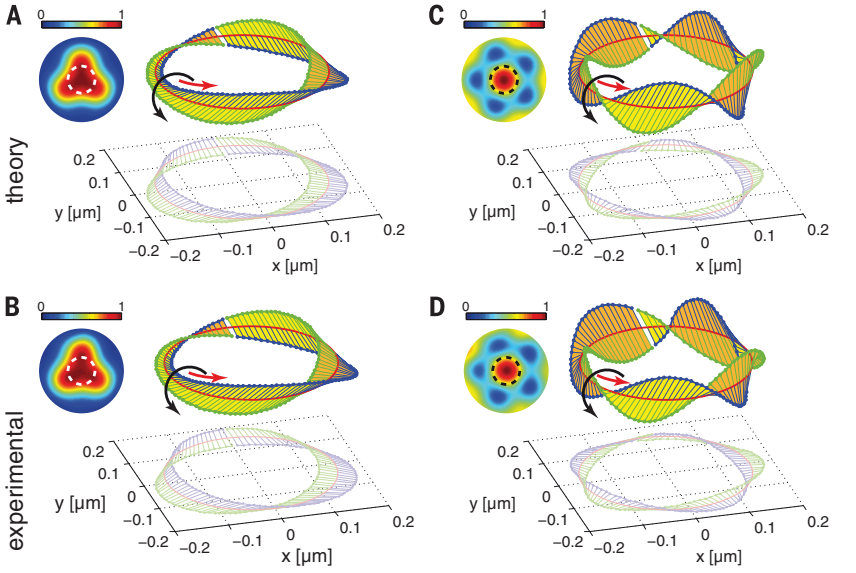

Fig. 3. Polarization topology of a highly nonparaxial Poincaré beam with topological charges of −1/2 and −3/2. (**A** and **C**) The numerically calculated polarization topologies in the focal plane of the beam. (**B** and **D**) The experimentally observed polarization topologies in the focal plane of the beam. Our experiment was performed under tight-focusing (nonparaxial) conditions, which accentuates the 3D topology of these Poincaré beams. In these plots, the major axis of the 3D polarization ellipse is represented as a function of position on a circle of 150 nm radius centered on the beam axis. This circle is shown as a dashed white or black line in the top-left insets superimposed to the scanned intensity image. In order to make the twist of the Möbius strip more noticeable, one half of the major axis of the local polarization ellipse is colored blue, and the other half is colored green. For a charge of −1/2 [(A) and (B)], we observe three half twists; for a charge of −3/2 (C and D), we observe five half twists. At the bottom of (A) to (D), the projection of the polarization major axis onto a plane (the *x*–*y* plane) transverse to the propagation direction *z* is shown.

ellipse around the optical axis (C-point). In this notation, the major and minor axes of the polarization ellipse and the normal to the polarization ellipse in the complex representation of the electric field are described by the vectors

$$\alpha = \frac{1}{\left|\sqrt{\mathbf{E}\cdot\mathbf{E}}\right|}\Re(\mathbf{E}^*\sqrt{\mathbf{E}\cdot\mathbf{E}})$$
$$\beta = \frac{1}{\left|\sqrt{\mathbf{E}\cdot\mathbf{E}}\right|}\Im(\mathbf{E}^*\sqrt{\mathbf{E}\cdot\mathbf{E}}) \quad , \qquad (2)$$
$$\gamma = \Im(\mathbf{E}^*\times\mathbf{E})$$

where $\Re(\mathbf{E})$, $\Im(\mathbf{E})$, and $\mathbf{E}^*$ represent the real and imaginary parts of $\mathbf{E}$ and its complex conjugate, respectively. In this representation, a C-line is a trajectory of $\mathbf{r}$ upon propagation in which the major and minor axes of the ellipse become degenerate, $\boldsymbol{\alpha}(\mathbf{r}) = \boldsymbol{\beta}(\mathbf{r}) = 0$. In our case, as the beam propagates, the polarization ellipses change in the transverse plane because TEM_{00} and $LG_{0,\pm1}$ possess different Gouy phases (*8*). The polarization topology of the beam remains unchanged but undergoes a global rotation that depends on the propagation distance. Furthermore, the C-line coincides with the optical axis in this case. In order to visualize and plot the polarization topology in 3D space, we considered only the polarization configuration in a plane orthogonal to the C-line, which is known as the principal plane. In particular, we considered first the focal plane, where the field's *z*-component is largest. We then calculated the major and minor ($\boldsymbol{\alpha}$, $\boldsymbol{\beta}$) axes of the polarization ellipses at all points lying on a circle in the principal plane, with the C-point in its center.

Because a strong longitudinal component of the electric field is generated, the major axis $\boldsymbol{\alpha}$ of the polarization ellipse undergoes a twist out of the focal plane in 3D space and forms a Möbius strip. The twisting direction for the specific topology under study is clockwise, which indicates a positive polarization topological charge of 3/2, or three half-twists. We show the corresponding theoretically calculated and experimentally observed Möbius strips with 3/2-twists for a Poincaré beam with $q = -1/2$ under tight focusing in Fig. 3, A and B, respectively. A Möbius strip of 5/2-twists is created and also observed by replacing the *q*-plate of $q = -1/2$ with one of $q = -3/2$. The corresponding theoretically expected and experimentally measured Möbius strips are shown in Fig. 3, C and D, whereas the focal field distributions are presented in the supplementary materials (*10*). Our measurements were performed in the focal plane, but the Möbius structure extends outside of the focal plane and for a variety of radii; additional results are given in the supplementary materials (*10*).

Our results reveal a hidden polarization topology under tight focusing that has not previously been reported in literature. These results are relevant to fundamental studies of optics and physics, light coupling to nanostructures, light-matter interactions, and nano-optics (*30*–*32*). Optical patterns such as those we demonstrate here could, for example, be used to optically fabricate material microstructures with nontrivial topology for new functional media—for example, metamaterials with exotic optical properties or molecular-shape–selective membranes or substrates.

REFERENCES AND NOTES

1. J. F. Nye, M. V. Berry, *Proc. R. Soc. Lond., Math. Phys. Sci.* **336**, 165–190 (1974).
2. J. F. Nye, *Natural Focusing and Fine Structure of Light: Caustics and Wave Dislocations* (CRC Press, Boca Raton, FL, 1999).
3. I. V. Basistiy, M. S. Soskin, M. V. Vasnetsov, *Opt. Commun.* **119**, 604–612 (1995).
4. J. Leach, M. R. Dennis, J. Courtial, M. J. Padgett, *Nature* **432**, 165 (2004).
5. M. R. Dennis, R. P. King, B. Jack, K. O'Holleran, M. J. Padgett, *Nat. Phys.* **6**, 118–121 (2010).
6. F. Flossmann, K. O'Holleran, M. R. Dennis, M. J. Padgett, *Phys. Rev. Lett.* **100**, 203902 (2008).
7. E. J. Galvez, S. Khadka, W. H. Schubert, S. Nomoto, *Appl. Opt.* **51**, 2925–2934 (2012).
8. F. Cardano, E. Karimi, L. Marrucci, C. de Lisio, E. Santamato, *Opt. Express* **21**, 8815–8820 (2013).
9. M. V. Berry, J. H. Hannay, *J. Phys. Math. Gen.* **10**, 1809–1821 (1977).
10. More details on 2D polarization topologies, *q*-plate output beams, and mode analysis, as well as the reconstruction technique and 3D polarization distribution through the focal volume, can be found in the supplementary materials.
11. A. E. Siegman, *Lasers* (University Science Books, Herndon, VA, 1986).
12. A. M. Beckley, T. G. Brown, M. A. Alonso, *Opt. Express* **18**, 10777–10785 (2010).
13. M. R. Dennis, K. O'Holleran, M. J. Padgett, *Prog. Opt.* **53**, 293–363 (2009).
14. I. Freund, *Opt. Commun.* **283**, 1–15 (2010).
15. I. Freund, *Opt. Commun.* **249**, 7–22 (2005).
16. I. Freund, *Opt. Lett.* **35**, 148–150 (2010).
17. C. A. Pickover, *The Möbius Strip: Dr. August Möbius's Marvelous Band in Mathematics, Games, Literature, Art, Technology, and Cosmology* (Thunder's Mouth Press, New York, 2005).
18. E. L. Starostin, G. H. M. van der Heijden, *Nat. Mater.* **6**, 563–567 (2007).
19. D. J. Craik, *Toxicon* **39**, 1809–1813 (2001).
20. A. Ynnerman, S. C. Chapman, P. Ljung, N. Andersson, *IEEE Trans. Plasma Sci.* **30**, 18–19 (2002).
21. C.-W. Chang *et al.*, *Phys. Rev. Lett.* **105**, 259903 (2010).
22. S. Tanda *et al.*, *Nature* **417**, 397–398 (2002).
23. T. Machon, G. P. Alexander, *Proc. Natl. Acad. Sci. U.S.A.* **110**, 14174–14179 (2013).
24. L. Marrucci, C. Manzo, D. Paparo, *Phys. Rev. Lett.* **96**, 163905 (2006).
25. S. Slussarenko *et al.*, *Opt. Express* **19**, 4085–4090 (2011).
26. B. Richards, E. Wolf, *Proc. R. Soc. London Ser. A* **253**, 358–379 (1959).
27. T. Bauer, S. Orlov, U. Peschel, P. Banzer, G. Leuchs, *Nat. Photonics* **8**, 23–27 (2014).
28. Y. Zhao, J. S. Edgar, G. D. M. Jeffries, D. McGloin, D. T. Chiu, *Phys. Rev. Lett.* **99**, 073901 (2007).
29. M. V. Berry, *J. Opt. A, Pure Appl. Opt.* **6**, 675–678 (2004).
30. A. Ambrosio, L. Marrucci, F. Borbone, A. Roviello, P. Maddalena, *Nat. Commun.* **3**, 989 (2012).
31. K. Toyoda, K. Miyamoto, N. Aoki, R. Morita, T. Omatsu, *Nano Lett.* **12**, 3645–3649 (2012).
32. K. Sugioka, Y. Cheng, *Light Sci. Appl.* **3**, e149 (2014).

ACKNOWLEDGMENTS

The authors thank C. Marquardt for fruitful discussions. E.K. and R.W.B. acknowledge the support of the Canada Excellence Research Chairs (CERC) Program.

SUPPLEMENTARY MATERIALS

www.sciencemag.org/content/347/6225/964/suppl/DC1
Materials and Methods
Supplementary Text
Figs. S1 to S6
References (*33*–*35*)

1 September 2014; accepted 16 January 2015
Published online 29 January 2015;
10.1126/science.1260635